UNIVERSITE BLAISE PASCAL IN2P3/CNRS

LABORATOIRE DE PHYSIQUE CORPUSCULAIRE

63177 AUBIERE CEDEX TELEPHONE : 73 40 72 72

TELECOPIE : 73 26 45 98

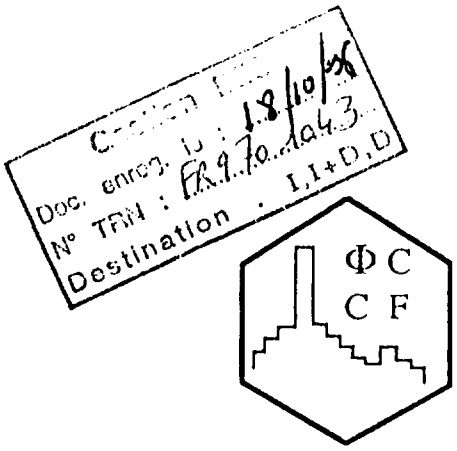

OUT- OF -PLANE EMISSION OF NUCLEAR MATTER IN AU + AU COLLISIONS BETWEEN 100 AND 800 AMEV

Bastid N., Buta A., Crochet P., Dupieux P., Petrovici M., Rami F., Alard J.P., Amouroux V., Basrak Z., Belyaev I., Best D., Biegansky J., Blaich T., Caplar R., Cerruti C., Cindro N., Coffin J.P., Dona R., Dzelalija M., Erö E., Fan Z.G., Fintz P., Fodor Z., Fraysse L., Freifelder R.P., Gobbi A., Guillaume G., Herrmann N., Hildenbrand K.D., Hölbling S., Hong B., Jeong S.C., Jundt F., Keczkemeti J., Kirejczyk M., Konez P., Korchagin Y., Kotte R., Krämer M., Kuhn C., Lebedev A., Legrand I., Leifels Y., Maazouzi C., Manko V., Mgebrishvili G., Moisa D., Mösner J., Neubert W., Pelte D., Pinkenburg C., Pras P., Reisdorf W., Ritman J.L., Roy C., Sadchikov A.G., Schüll D., Seres Z., Sikora B., Simion V., Siwek-Wilczynska K., Smolyankin V., Sodan U., Teh K.M., Tizniti L., Trzaska M., Vasiliev M., Wagner P., Wang G.S., Wessels J.P., Wienold T., Wisniewski K., Wohlfarth D., Zhilin A.

Laboratoire de Physique Corpusculaire de Clermont-Ferrand
IN2P3/CNRS - Université Blaise Pascal
F-63177 AUBIERE Cedex, France
Centre de Recherches Nucléaires, IN2P3/CNRS - Université Louis Pasteur
67037 STRASBOURG Cedex 02, France
Inst. for Physics and Nuclear Engineering
BUCHAREST - Romania

and

FOPI Collaboration

PCCF RI 9604

Out – of – Plane Emission of Nuclear Matter in Au + Au Collisions between 100 and 800 AMeV

N. Bastid[1], A. Buta[2], P. Crochet[3], P. Dupieux[1], M. Petrovici[2], F. Rami[3], J.P. Alard[1], V. Amouroux[1], Z. Basrak[13], I. Belyaev[10], D. Best[5], J. Biegansky[6], T. Blaich[9], R. Čaplar[13], C. Cerruti[3], N. Cindro[13], J.P. Coffin[3], R. Donà[8], M. Dželalija[13], E. Erö[4], Z.G. Fan[5], P. Fintz[3], Z. Fodor[4], L. Fraysse[1], R.P. Freifelder[5], A. Gobbi[5], G. Guillaume[3], N. Herrmann[5,7], K.D. Hildenbrand[5], S. Hölbling[13], B. Hong[5], S.C. Jeong[5], F. Jundt[3], J. Keczkemeti[4], M. Kirejczyk[12], P. Koncz[4], Y. Korchagin[10], R. Kotte[6], M. Krämer[5], C. Kuhn[3], A. Lebedev[10,11], I. Legrand[2], Y. Leifels[5], C. Maazouzi[3], V. Manko[11], G. Mgebrishvili[11], D. Moisa[2], J. Mösner[6], W. Neubert[6], D. Pelte[7], C. Pinkenburg[5], P. Pras[1], W. Reisdorf[5], J.L. Ritman[5], C. Roy[3], A.G. Sadchikov[11], D. Schüll[5], Z. Seres[4], B. Sikora[12], V. Simion[2], K. Siwek-Wilczynska[12], V. Smolyankin[10], U. Sodan[5], K.M. Teh[5], L. Tizniti[3], M. Trzaska[7], M. Vasiliev[11], P. Wagner[3], G.S. Wang[5], J.P. Wessels[5], T. Wienold[5], K. Wisniewski[12], D. Wohlfarth[6], A. Zhilin[10]

FOPI Collaboration

[1] *Laboratoire de Physique Corpusculaire, IN2P3-CNRS, Université Blaise Pascal, Clermont-Fd, France*

[2] *Institute for Physics and Nuclear Engineering, Bucharest, Romania*

[3] *Centre de Recherches Nucléaires, IN2P3-CNRS, Université Louis Pasteur, Strasbourg, France*

[4] *Research Institute for Particles and Nuclear Physics, Budapest, Hungary*

[5] *Gesellschaft für Schwerionenforschung, Darmstadt, Germany*

[6] *Forschungszentrum Rossendorf, Dresden, Germany*

[7] *Physikalisches Institut der Universität Heidelberg, Heidelberg, Germany*

[8] *Istituto Nazionale di Fisica Nucleare, Legnaro, Italy*

[9] *Universität Mainz, Mainz, Germany*

[10] *Institute for Theoretical and Experimental Physics, Moscow, Russia*

[11] *Russian Research Institute "Kurchatov", Moscow, Russia*

[12] *Institute of Experimental Physics, Warsaw University, Warsaw, Poland*

[13] *Rudjer Boskovic Institute, Zagreb, Croatia*

Abstract

We present new experimental results concerning the azimuthal distributions of light and intermediate mass fragments at midrapidity for Au (100 – 800 AMeV) + Au collisions measured with the phase I setup of the FOPI detector at GSI in Darmstadt. The azimuthal distributions are investigated as a function of the collision centrality, the incident energy, the fragment charge and transverse momentum. The maximum of the azimuthal anisotropy is obtained for collisions associated with impact parameters around 7 fm. Intermediate mass fragments present a stronger out-of-plane emission signal than light fragments. We show in particular that the azimuthal anisotropy as a function of the scaled fragment transverse momentum follows an universal curve for incident energies ranging from 250 to 800 AMeV. A signature for a transition from in-plane to out-of-plane emission is evidenced at the lowest beam energies.

PACS : 25.70.-z, 25.70.Pq

Keywords : Nuclear reactions ^{197}Au (^{197}Au, X), E = 100 to 800 AMeV ; out-of-plane emission; azimuthal anisotropy versus collision centrality, fragment charge and transverse momentum, incident energy ; scaling ; transition energy.

I- Introduction

One of the main motivations of relativistic heavy ion collisions is the possibility to create a hot and dense participant region which can be used to obtain information on the nuclear equation of state. Collective flow effects play an important role in extracting this kind of information [1, 2]. The in-plane flow component has been intensively studied in previous works [3 – 10]. In this paper, we focus on the preferential emission of particles in the direction perpendicular to the reaction plane. Such an analysis presents a great interest because it is the only direction where the nuclear matter might escape without being rescattered by either the target or projectile remnants and thus a less disturbed information on the matter of high density and temperature is expected. Moreover, the azimuthal distributions are expected to be strongly influenced by the nuclear equation of state [2, 11 – 13]. This out-of-plane emission of nuclear matter has been predicted by hydrodynamical calculations [14 – 16] and investigated in detail by various microscopic model calculations [11, 12]. Experimental evidence was first presented by the Diogène Group for proton-like particles [17] then by the Plastic Ball Group for light particles [18]. Recent experimental results concerning pions [19 – 21], neutrons [22, 23] and light particles [24, 25] have been also obtained.

We extend the analysis for the first time to intermediate mass fragments which are expected to exhibit a strong sensitivity to collective motion. The out-of-plane emission of nuclear matter at midrapidity is studied by means of azimuthal distributions around the beam axis, with respect to the reaction plane. The flow axis is not used as polar axis because of the limited acceptance of the phase I of the FOPI detector.

The anisotropy of azimuthal distributions, measured for semi-central and central Au on Au collisions in the incident energy range 100 – 800 AMeV with the phase I FOPI detector [26], is investigated as a function of the collision centrality, the incident energy, the fragment charge and transverse momentum. The maximum of the azimuthal anisotropy is extracted from semi-central collisions. Intermediate mass fragments reveal a higher sensitivity to collective motion than light fragments. The out-of-plane emission signal depends on the fragment transverse momentum. For incident energies from 250 to 800 AMeV the azimuthal anisotropy is independent of the bombarding energy if plotted versus the fragment transverse momentum scaled with the projectile center of mass momentum. A continuous evolution of the azimuthal distributions from in-plane (rotation-like behaviour) to out-of-plane emission is evidenced as a function of the incident energy. The incident energy at which this transition takes place is determined.

II- Experimental setup

The data for Au + Au collisions at incident energies ranging from 100 to 800 AMeV were obtained during experiments performed with the phase I of the FOPI detector [26] at the SIS/ESR accelerator facility of GSI – Darmstadt. This setup covered the laboratory polar angles 1.2^0 to 30^0 with full azimuthal coverage. It consists of a highly segmented Forward Wall of 764 plastic scintillators, each of them providing an energy loss and a time-of-flight signal hence determining the element number Z

and the velocity of charged particles. This plastic wall is divided in two parts : the Inner Wall (252 trapezoidal scintillator paddles) covers polar angles from 1.2^0 to 7.5^0 and the External Wall (512 scintillator strips) polar angles from 7^0 to 30^0. In order to achieve low detection thresholds and to extend the element identification up to Z = 15, the whole wall is covered by a shell of 188 thin energy loss detectors (cluster detectors) consisting of an ensemble of gas-filled ionization chambers (Parabola) in front of the External Wall and thin plastic scintillator paddles (Rosace) in front of the Inner Wall. An helium-filled bag is placed between the target and the Forward Wall. With this setup charge identification up to Z = 15 is obtained, with energy thresholds in the external part of the detector increasing from 14 AMeV for Z = 1 fragments to 50 AMeV for Z = 15 fragments. The energy thresholds are slightly higher in the inner part due to larger flight path and larger thickness of the Rosace paddles in comparison to the Parabola ionization chambers.

An example of the detector acceptance is presented in figure 1 for the Au on Au reaction at 250 AMeV in a normalized transverse momentum $P_0^{\perp}$ versus reduced rapidity y_0 plane ($P_0^{\perp} = (P^{\perp}/A)/(P_P/A_P)^{cm}$ where $(P_P/A_P)^{cm}$ is the projectile momentum per nucleon in the center-of-mass system and $y_0 = (y - y_{cm})/y_{cm}$, y_{cm} being the center-of-mass rapidity). This figure contains the angular limits at 1.2^0 and 30^0 and the shadows introduced by the Parabola frame (only for experiments performed between 100 - 400AMeV). The dashed vertical line at $y_0 = 0$ separates the forward and backward hemisphere in the collision of this symmetrical system. The detection thresholds for Z = 6 fragments are also plotted in the figure. The box illustrates the cuts introduced in most analyses performed between 150 - 800 AMeV.

The most important generated triggers are derived from the multiplicity of charged particles in the External Wall (PM). The minimum bias trigger requires a multiplicity PM $\geq$ 4 while for the central trigger this multiplicity is adjusted to a value which permits to select impact parameters less than 9 fm in a clean-cut geometrical model.

III- Analysis method

A- Centrality selection

Exclusive experiments permit to define global observables on an event basis which can be used to select an impact parameter range. For event characterization several variables have been intensively studied in the FOPI collaboration. The first one is the multiplicity of charged particles measured in the External Wall (PM) [27]. The distribution shows the well known flat plateau and falls off steeply at higher multiplicities. The highest multiplicity bin (PM5) starts at half the plateau value corresponding to an integrated cross section of about 100 mb. The remaining multiplicity range is divided into four equally spaced intervals PM1 to PM4. The multiplicity range PM3 to PM5 corresponds approximately to the central trigger events, with a negligible level of background. Most of the analyses presented in this report are obtained with this trigger condition.

It turns out that the PM5 criterion is not sufficient to select highly central events with an impact parameter b $\leq$ 1 - 2 fm. So, the other observable which has been used

to sort events is the stopping variable ERAT [28]. The variable ERAT is defined as the ratio of the transversal to the longitudinal kinetic energy in the forward hemisphere of the center of mass system :

$$\mathrm{ERAT} = \left. \frac{\sum_i E_i^{\perp}}{\sum_i E_i^{//}} \right\}_{y \geq y_{cm}} \quad (1)$$

Large ERAT values correspond to events associated with a large transfer of longitudinal energy into transverse energy indicating more central collisions whereas small ERAT values can be assigned to more peripheral collisions. The highest ERAT cut (ERAT5), with the same integrated cross section as in PM5, succeeds to select rather central events associated with a high degree of stopping. The remaining normalized distribution is then divided into 5 equally spaced intervals ERAT0 to ERAT4. The regions ERAT0 and ERAT1 are strongly affected by the central trigger cut. With the ERAT5 selection a pronounced source of intermediate mass fragments is evidenced at midrapidity. In the following we use these two global observables. We show in figure 2, for Au + Au collisions at 400 AMeV, the impact parameter selecting power of theses variables predicted by the dynamical "Isospin" QMD model (IQMD) [12, 29] with the HM parametrization (hard skyrme potential supplemented with a momentum dependent interaction). Simulated events have been filtered through the experimental FOPI filter. The simulation indicates clearly that ERAT provides a better cut on central collisions (for impact parameters b $\leq$ 5 fm) than PM does. A strong correlation between ERAT and the impact parameter is observed in this case. For larger impact parameters the global variable PM is more effective than ERAT. These results explain in particular the choice of PM to extract the maximum of the out-of-plane emission

(see section IV). We give also in table 1 the mean value of the impact parameter distribution and the corresponding dispersion for the event classes ERAT2 to ERAT5 and PM3 to PM5. Similar trends have been also observed for other incident energies.

B- Reaction plane determination and azimuthal distribution parametrization

We report on azimuthal distributions of light and intermediate mass fragments at midrapidity, around the beam axis with respect to the reaction plane. The azimuthal angle between the emitted particle (φ) and the reaction plane (φ_r) $\varphi' = \varphi - \varphi_r$ is estimated by first calculating event by event the azimuthal orientation of the reconstructed reaction plane, applying the standard transverse momentum analysis [30]. In order to get an estimation of the accuracy on the reaction plane determination we calculate $< \cos\Delta\varphi_r >$, $\Delta\varphi_r$ being a measure of the deviation to the true reaction plane as the so-called true reaction plane is not known. In the method described in [30] this quantity is estimated by randomly subdividing each event into two subevents of the same multiplicity. The mean of the experimental $\cos(\frac{\varphi_1 - \varphi_2}{2})$ distribution, where $\varphi_1 - \varphi_2$ is the azimuthal angle between the two subevent reaction planes, is an estimate for $< \cos\Delta\varphi_r >$. Simulations with the IQMD model, in which the true reaction plane is known, show that the method does not give accurate results for low multiplicity event classes. In these cases $< \cos\Delta\varphi_r >$ values have been determined with the IQMD model and thus $< \cos\Delta\varphi_r > = < \cos(\varphi_{true} - \varphi_{est}) >$, φ_{true} and φ_{est} being respectively the azimuthal angle of the true and estimated reaction plane. The

lowest $< \cos\Delta\varphi_r >$ values are obtained for the lowest incident energies or for the more central or peripheral collisions. Concerning the analyses which are presented in this report, $< \cos\Delta\varphi_r >$ values vary approximately between 0.70 and 0.95. A high value implies, of course, a better determination of the reaction plane since $< \cos\Delta\varphi_r > = 1$ in the limiting case of zero dispersion.

The same procedure is used to calculate the $< \cos^2\Delta\varphi_r >$ values needed to correct a'_2 and R'_N coefficients for finite number effects.

The azimuthal distributions will be parametrized by Fourier series :

$$\frac{dN}{d\varphi'} = a'_0 \left(1 + a'_1 \cos\varphi' + a'_2 \cos 2\varphi' \right) \qquad (2)$$

a'_0 is a normalization factor, a'_1 is related to the in-plane flow component and a'_2 to the out-of-plane flow component. a'_2 is negative for an out-of-plane enhancement, equal to zero for an uniform distribution and positive for an in-plane emission. In order to quantify the out-of-plane anisotropic emission the results can be summarized in terms of the out-of-plane emission ratio R'_N. R'_N is defined as the ratio of the number of particles emitted perpendicularly to the reaction plane to the number of particles emitted in the reaction plane :

$$R'_N = \frac{N(90^0) + N(-90^0)}{N(0^0) + N(180^0)} = \frac{1 - a'_2}{1 + a'_2} \qquad (3)$$

A value of R'_N greater than 1 corresponds to a preferential out-of-plane emission.

We have restricted the analysis to a narrow region around the center of mass rapidity where flow effects are small. All the results presented in the incident energy

range 150 to 800 AMeV are obtained by applying the condition $-0.15 < y_0 < 0.15$ (figure 1). The lowest limit, $y_0 > -0.15$, is mainly dictated by the detector energy cut. For the 100 AMeV, a more severe cut has been applied (see section VII). We have checked that the parameter R'_N does not vary if we slightly modify the y_0 condition (depends only on the fragment transverse momentum cut).

The R'_N parameters have been corrected for finite number effects. The corrected quantity R_N [31] is given by :

$$R_N = \frac{1 - a_2}{1 + a_2} \text{ with } a_2 = \frac{a'_2}{2 < \cos^2 \Delta\varphi_r > - 1} \tag{4}$$

C- Azimuthal distributions and apparatus response

The figure 3 shows an example of azimuthal distributions obtained at 800 AMeV. The collisions have been selected with the ERAT criterion. In addition to the condition on the reduced rapidity, we have applied a cut on the normalized fragment transverse momentum : $0.06 < P_0^{\perp} < 0.48$. With this rectangular and symmetrical window in the ($P_0^{\perp}$, y_0) plane (figure 1), in-plane flow effects should cancel out and thus a preferential emission in the direction perpendicular to the reaction plane can be observed directly in the figures (enhancement around $\varphi' = \pm 90^0$). For the 100 AMeV incident energy, which will be discussed in section VII, the cuts are different because of higher fragment detection thresholds.

From this figure we can extract the following characteristics. A clear signature of an out-of-plane signal is evidenced in the transverse momentum range of the FOPI

phase I acceptance. The top part of the figure shows the centrality dependence of the out-of-plane signal for Z = 2 fragments. The azimuthal anisotropy is strongest for intermediate impact parameters (event class ERAT2) and it decreases as the impact parameter decreases. A similar behaviour is observed for other Z. The bottom part of the figure depicts the fragment charge dependence of the out-of-plane emission signature for the event class ERAT2. The enhancement around $\varphi' = \pm 90^0$ increases with the charge of the detected fragments. These qualitative results can be generalized to the other incident energies down to 150 AMeV although the out-of-plane signal is weaker at the lowest energies (see later).

The influence of the experimental setup on the azimuthal distributions has been also studied from simulations with Au + Au IQMD events at 400 AMeV (HM parametrization, impact parameter range 0 - 7 fm). These events have been filtered through the FOPI filter, which takes into account the geometrical acceptance and the energy thresholds, and through the GEANT - FOPI filter. The latter includes the modular description of the detector and simulates also the double hit effects. Same cuts, as in the experimental data, are applied to y_0 and to $P_0^{\perp}$. Then the simulated azimuthal distributions are treated exactly as the data but only Z = 1 was used because of statistical limitations.

The R_N values given by the two filters are very close. The acceptance effects are clearly evidenced comparing the whole simulation (no $P_0^{\perp}$ cut) and the filtered simulation : a reduction of the out-of-plane emission signal is observed, the R_N values being smaller in the FOPI phase I acceptance (low transverse momentum values) than

in the 4π acceptance.

All these tests performed with simulations give us confidence in the extraction of the out-of-plane emission parameters from experimental φ' distributions.

IV- Centrality dependence of the azimuthal anisotropy

The results concerning the collision centrality dependence of the azimuthal anisotropy, obtained using the ERAT criterion (ERAT2 to ERAT5 bins), have shown that the anisotropy increases as the impact impact parameter increases. The largest R_N value is obtained for the ERAT2 bin which selects impact parameters around 7.4 fm. In order to see whether the maximum of the out-of-plane emission is reached for these intermediate impact parameters similar analyses have been performed with the minimum bias trigger events sampled with the PM criterion which exhibits a better correlation than ERAT with the large impact parameters (see figure 2). The results are summarized in figure 4 for Au on Au collisions at 400 AMeV and for proton-like particles (each detected particle is weighted by its charge). The data indicate a clear correlation between R_N and the multiplicity. The maximum of the out-of-plane emission is obtained for intermediate multiplicities which select impact parameters of about 7 fm. All these trends are also observed for other incident energies ranging from 250 AMeV to 800 AMeV and for different charged particles. Such a behaviour permits to deduce that the anisotropy is mainly caused by shadowing effects [2] of the spectator remnants which play a role during the expansion phase of the interaction

zone.

Similar findings were reported by the Plastic Ball Collaboration [18] for light particles and by the Land Collaboration for neutrons [23].

Concerning the sideward flow studies realized as a function of the collision centrality, the results from the FOPI collaboration [7 – 9, 32] show that the maximum is obtained for impact parameters around 3 – 4 fm.

V- Fragment charge dependence of the azimuthal anisotropy

The results of this study are displayed in figure 5 for Au on Au collisions at 250 AMeV selected with PM3. The anisotropy becomes more pronounced as the fragment charge increases, R_N increasing significantly from $Z = 1$ to $Z = 3$ and flattening-off for heavier fragments ($Z \geq 4$). This trend is observed for other incident energies ranging from 150 to 800 AMeV and centrality collision selections (see figure 6). This behaviour agrees qualitatively with recent IQMD predictions [12]. The result confirms the high sensitivity of the intermediate mass fragments to the collective motion while the light particles are more influenced by the thermal motion. The observed Z dependence of the azimuthal anisotropy is similar to the one characterizing the sideward flow [6] and has been also evidenced in the collective expansion observed in highly central collisions [33, 34].

The dependence of the out-of-plane emission signal as a function of the fragment charge can be understood from a simple picture of an expanding thermal source where

a pure collective motion is superimposed to the random thermal one [35, 36]. But the shadowing effects present after the expansion of the system explain the anisotropies observed in the azimuthal distributions.

VI- Incident energy and fragment transverse momentum dependence of the azimuthal anisotropy

The R_N values obtained for the centrality selection ERAT2 and different charged fragments emitted in Au on Au collisions are presented in figure 6 as a function of the bombarding energy in the incident energy range 150 – 800 AMeV. R_N increases significantly up to 250 AMeV for all charged fragments and levels off. The same behaviour is observed for other centrality selections. In order to study this trend in more detail the excitation function of R_N has been determined as a function of the fragment transverse momentum.

The results are reported in figure 7 for Z = 2 fragments and for the centrality selection ERAT2. First, a strong correlation of R_N with the transverse momentum is observed : R_N increases monotonously with this quantity. The left part of the figure shows that with increasing bombarding energy the out-of-plane signal is shifted to increasingly higher values of the transverse momentum per nucleon $P^{\perp}/A$. If we now consider the dependence of R_N versus $P_0^{\perp}$ (right part of the figure), an almost universal curve independent of the bombarding energy is obtained except for the 150 AMeV incident energy. This effect is also clearly observed for other fragments (in

particular for Z = 1 fragments) and impact parameters.

This particular behaviour referred to the scaling of $R_N(P_0^\perp)$ has been already observed by the LAND collaboration [23] and is confirmed by recent theoretical investigations [37] for neutrons which exhibit very similar trends as protons.

These results obey the scaling laws of non-viscous fluid dynamics [38]. A scaling behaviour has been already predicted for the sideward flow characterized by the flow parameter [39] : the slope of the curve $< p^x(y) >$ at $y = y_{cm}$, $< p^x(y) >$ being the mean transverse momentum in the reaction plane. It has been evidenced experimentally for Au (E/A = 150 - 800 MeV) + Au collisions [40].

We observe a break in the scaling of $R_N(P_0^\perp)$ for incident energies lower than 250 AMeV (figure 7). In this beam energy range, the out-of-plane enhancement is decreasing faster than a simple scaling law would predict with decreasing bombarding energy. In order to see whether we can confirm this trend and eventually give prominence to an in-plane enhancement (R_N values < 1), the 100 AMeV incident energy will be reported in the following part with particular cuts in the $(P_0^\perp, y_0)$ plane.

VII- Transition from in-plane to out-of-plane emission

At incident energies lower than 100 AMeV an in-plane enhancement was observed [41, 42]. A rotation motion of the participant zone was taken as an explanation of this type of alignment. At incident energies higher than 100 AMeV, as it was mentioned

before, the expansion of the hot and compressed participant matter, hindered by the presence of the projectile and target spectators, follows a squeeze-out pattern which in an azimuthal distribution is observed as an out-of-plane enhancement. Thus, besides the standard studies of the squeeze-out phenomenon as a function of impact parameter, rapidity, mass and transverse momentum, a detailed study of a possible transition from in-plane to out-of-plane emission as a function of incident energy in the midrapidity region could give more details on the relative contribution of the attractive and repulsive forces, the life-time of the emitting source, its rotational energy and expansion dynamics [43]. Comparisons with the IQMD calculations [12] show that the transition energy is an observable which could have a high selectivity on the compressibility value used in the models.

Due to threshold problems and restricted phase space coverage in our experiment [26] we limit the present analysis at Z = 2, 3 and 4 particles, at midrapidity region and in a region of normalized fragment transverse momenta, $P_0^{\perp}$ between 0.17 and 0.56 for which the symmetry relative to the center of mass exists for all incident energies starting from 100 AMeV. The rapidity region considered in these studies is $-0.1 < y_0 < 0.1$. The impact parameter selection was based on the multiplicity information delivered by the External Wall (PM). Detailed studies have been performed for two regions of impact parameter characterized by PM3 and PM4 which would correspond to semi-central and central events, respectively, but in the following only results for PM4, which selects impact parameters around 4 fm, will be shown.

Figure 8 shows the azimuthal distributions for the multiplicity bin PM4 and the lowest four incident energies measured. The three columns correspond to Z = 2,

3 and 4, respectively. The azimuthal distributions were fitted by the equation (2). These fits are shown in each figure by solid lines. The dashed curves show the $a'_1 cos\varphi'$ contribution and the dotted curves the contribution of the anisotropy term $a'_2 cos2\varphi'$. They are shifted vertically by multiplying a'_0 by 0.75 and 0.5 respectively. For the present analysis the a'_2 coefficient is of interest. A change of its sign from positive to negative values is indicative of an in-plane to out-of-plane transition of the azimuthal correlation. While for Z = 2, PM4, a clear reduction of the out-of-plane signal at 100 AMeV is observed, for Z = 4, PM4, the pattern of the azimuthal distribution and the obtained value of a'_2 coefficient suggest an in-plane alignment. For PM3 multiplicity selection, at 100 AMeV, for all types of fragments, Z = 2, 3 and 4, the distributions seem to be isotropic in azimuth. Whatever the centrality selections PM3 or PM4, the out-of-plane signal is increasing as a function of incident energy up to 250 AMeV and for higher incident energies the effect saturates as it was shown in the previous chapter.

In figure 9 R_N is represented as a function of incident energy for the three Z values analysed. As previously, a clear dependence of the out-of-plane emission signal on the charge of the analysed particle can be seen.

The transition energies from in-plane to out-of-plane enhancement in figure 9 (E-tran) have been determined as the intercept of $R_N = 1$ with a second order polynomial fit of each distribution. The errors associated to these energies (having only statistical origin) range from about 20% for Z = 2 and Z = 3 to 30% for Z = 4. These energies are sensibly higher than the balance energy E_{bal} for the vanishing of sideward flow in Au + Au collisions [44], estimated at about 60 AMeV. A similar conclusion

was obtained for $^{40}Ar + ^{51}V$ system [45] while for $^{64}Zn + ^{58}Ni$ system the reported E-tran values are lower than the E_{bal} values [46, 47]. As it was mentioned in section III-B the present studies have been done using azimuthal distributions around the beam axis relative to the reaction plane, imposed by the phase space coverage of the phase I of our device. This explains why these studies have been restricted to a narrow region around midrapidity where the influence of the sideward flow on extracted E-tran values is negligible.

In order to study the effect of the experimental device on this transition energy, a similar analysis has been performed with the IQMD model [12, 29]. As for experimental data, we observe for non-filtered IQMD data the same evolution with the incident energy ; namely, both versions of IQMD calculations, HM (stiff equation equation of state plus momentum dependent interaction) and SM (soft equation of state plus momentum dependent interaction) present an in-plane to out-of-plane transition in the azimuthal distribution around 120 and 110 AMeV, respectively. These values, using the above fitting procedure, can be determined with an accuracy of about 30% due to the present available statistics of the generated events. Due to lack of statistics, these studies have been limited to Z = 2 particles. The threshold effects superimposed on the geometrical acceptance diminish the out-of-plane signal. This effect is different for the two sets of generated data. While the out-of-plane emission ratio is slightly higher for non-filtered HM data, the situation for filtered events at higher incident energies, as it is seen in figure 9, is reversed. Nevertheless, the influence on the transition energy is negligible ; the values for the filtered events being 121 and 104 AMeV, for HM and SM respectively, agree with the above values of the transition energies for non-filtered

data within statistical errors. In figure 9 we show with empty triangles and empty circles the results of these calculations for filtered generated events, for SM and HM respectively. As it could be seen in this figure, a better agreement with the measured out-of-plane ratio is obtained using a stiff equation of state. As far as concerns the transition energy, within the limit of statistical errors, both versions give a fair good agreement with the experiment.

VIII- Conclusion

We have presented new experimental results concerning the out-of-plane emission at midrapidity of light and intermediate mass fragments emitted in the angular range 1.2^0 - 30^0 in Au + Au collisions between 100 and 800 AMeV. We have shown that the effect is enhanced for intermediate mass fragments and for collisions associated with intermediate impact parameters (b $\simeq$ 7 fm). The magnitude of the signal depends on the transverse momentum of the observed particles. A scaling has been found in the incident energy range 250 to 800 AMeV (R_N versus the normalized transverse momentum $P_0^{\perp}$ leads to an universal curve independent of the incident energy). The present studies show a continuous evolution from nearly isotropic or in-plane (rotation-like) behaviour to an out-of-plane enhancement as a function of incident energy. This transition energy could become a powerful variable in studying the relative contributions of the attractive and repulsive forces, the life-time of the emitting source, its rotational motion and expansion dynamics.

All these analyses will be extended to particles emitted in the whole acceptance of the complete FOPI detector [48]. The studies will concern the data obtained from the experiments performed with Au + Au, Ni + Ni, Xe + CsI systems for incident energies ranging from 90 to 400 AMeV. For these data an isotopic separation will be possible above 30^0. Then the out-of-plane emission signal could be investigated as a function of the collision centrality, the bombarding energy, the target - projectile system, the particle mass and transverse momentum.

References

[1] : G. Peilert, H. Stöcker, W. Greiner, A. Rosenhauer, A. Bohnet, J. Aichelin, Phys. Rev. C39 (1989) 1402.

[2] : J. Aichelin, Phys. Rep. 202 (1991) 233.

[3] : R. E. Renfordt, D. Schall, R. Bock, R. Brockmann, J.W. Harris, A. Sandoval, R. Stock, H. Ströbele, D. Bangert, W. Rauch, G. Odyniec, H.G. Pugh, L.S. Schroeder, Phys. Rev. Lett. 53 (1984) 763.

[4] : H.A. Gustafsson, H.H. Gutbrod, J. Harris, B.V. Jacak, K.H. Kampert, B. Kolb, A.M. Poskanzer, H.G. Ritter, H.R. Schmidt, Mod. Phys. Lett. A3 (1988) 1323.

[5] : J. Gosset, M. Demoulins, R. Babinet, C. Cavata, H. Fanet, D. L'Hôte, B. Lucas, J. Poitou, O. Valette, M.C. Lemaire, J.P. Alard, J. Augerat, N. Bastid, P. Charmensat, P. Dupieux, L. Fraysse, J. Marroncle, G. Montarou, M.J. Parizet, D. Qassoud, A. Rahmani, F. Brochard, P. Gorodetzky, C. Racca, Phys. Lett. B247 (1990) 233.

[6] : F. Rami, R. Donà, C. Cerruti, J.P. Coffin, P. Fintz, G. Guillaume, A. Houari, F. Jundt, C. Kuhn, P. Wagner and the FOPI collaboration, GSI Report 93-1 (1993) p. 40.

[7] : T. Wienold, thesis, Heidelberg University, GSI Report 93-28 (1993).

[8] : FOPI collaboration, T. Wienold et al., GSI Report 94-74 (1994).

[9] : FOPI collaboration, V. Ramillien, P. Dupieux et al., Nucl. Phys. A587 (1995) 802.

[10] : EOS collaboration, M.D. Partlan et al., Phys. Rev. Lett. 75 (1995) 2100.

[11] : G.M. Welke, M. Prakash, T.T.S. Kuo, S. Das Gupta, C. Gale, Phys. Rev C38 (1988) 2101.

[12] : C. Hartnack, J. Aichelin, H. Stöcker, W. Greiner, Phys. Lett. B336 (1994) 131.

[13] : C. Hartnack, M. Berenguer, A. Jahns, A.V. Keitz, R. Mattiello, A. Rosenhauer, J. Schaffner, T. Schönfeld, H. Sorge, L. Winckelmann, H. Stöcker, W. Greiner, Nucl. Phys. A538 (1992) 53c.

[14] : W. Scheid, H. Müller, W. Greiner. Phys. Rev. Lett. 32 (1974) 741.

[15] : J. Kapusta and D. Strottman, Phys. Lett. B106 (1981) 33.

[16] : H. Stöcker, L.P. Csernai, G. Graebner, G. Buchwald, H. Kruse, R.Y. Cusson, J.A. Maruhn, W. Greiner, Phys. Rev. C25 (1982) 1873.

[17] : M. Demoulins, D. L'Hôte, J.P. Alard, J. Augerat, R. Babinet, N. Bastid, F. Brochard, C. Cavata, N. De Marco, P. Dupieux, H. Fanet, Z. Fodor, L. Fraysse, P. Gorodetsky, J. Gosset, T. Hayashino, M.C. Lemaire, A. Lemerdy, B. Lucas, J. Marroncle, G. Montarou, M.J. Pariset, J. Poitou, C. Racca, W. Schimmerling, Y. Terrien, O. Valette, Phys. Lett. B241 (1990) 476.

[18] : H.H. Gutbrod, K.H. Kampert, B. Kolb, A.M. Poskanzer, H.G. Ritter, R. Schicker, H.R. Schmidt, Phys. Rev. C42 (1990) 640.

[19] : TAPS collaboration, L. Venema et al., Phys. Rev. Lett. 71 (1993) 835.

[20] : C. Pinkenburg, thesis, Heidelberg University (1995).

[21] : KAOS collaboration, D. Brill et al., Phys. Rev. Lett. 71 (1993) 336.

[22] : LAND collaboration, Y. Leifels et al., Phys. Rev. Lett. 71 (1993) 963.

[23] : LAND collaboration, D. Lambrecht et al., Z. Phys. A350 (1994) 115.

[24] : KAOS collaboration, D. Brill et al, submitted to Z. Phys. A.

[25] : EOS collaboration, S. Wang et al., to be published.

[26] : FOPI collaboration, A. Gobbi et al., N.I.M. A324 (1993) 156.

[27] : FOPI collaboration, J.P. Alard et al., Phys. Rev. Lett. 69 (1992) 889.

[28] : W. Reisdorf for the FOPI Collaboration, Proceedings of the XX International Workshop on Gross Properties of Nuclei and Nuclear Excitations, Hirschegg, Austria, 1992, ed. H. Feldmeier (GSI Darmstadt) p. 38.

[29] : C. Hartnack, GSI report 93-05 (1993).

[30] : P. Danielewicz and G. Odyniec, Phys. Lett. B157 (1985) 146.

[31] : M. Demoulins, thesis, Paris-Sud University (1989).

[32] : R. Donà, F. Rami, C. Cerruti, J.P. Coffin, P. Fintz, G. Guillaume, A. Houari, F. Jundt, C. Kuhn, P. Wagner and the FOPI collaboration, GSI report 94-1 (1994) p. 19.

[33] : FOPI collaboration, S.C. Jeong et al., Phys. Rev. Lett. 72 (1994) 3468.

[34] : FOPI collaboration, M. Petrovici et al., Phys. Rev. Lett., 74 (1995) 5001.

[35] : P. Crochet, R. Donà, F. Rami, R. Kotte, C. Cerruti, J.P. Coffin, P. Fintz, G. Guillaume, F. Jundt, C. Kuhn, C. Maazouzi, C. Roy, L. Tizniti, P. Wagner and the FOPI collaboration, GSI report 95-1 (1995) p. 51.

[36] : P. Crochet, F. Rami, C. Cerruti, J.P. Coffin, P. Fintz, G. Guillaume, F. Jundt, C. Kuhn, C. Maazouzi, C. Roy, L. Tizniti, P. Wagner and the FOPI collaboration, GSI report 95-1 (1995) p. 55.

[37] : S.A. Bass, C. Hartnack, H. Stöcker, W. Greiner, Z. Phys A352 (1995) 171.

[38] : N. L. Balazs, B. Schürmann, K. Dietrich, L.P. Csernai, Nucl. Phys. A424 (1984) 605.

[39] : A. Bonasera, L.P. Csernai, B. Schürmann, Nucl. Phys. A476 (1988) 159.

[40] : R. Donà, thesis, Padova University (1994).

[41] : C.B. Chitwood, D.J. Fields, C.K. Gelbke, D.R. Klesh, W.G. Lynch, M.B. Tsang, T.C. Awes, R.L. Fergusson, F.E. Obenshain, F. Plasil, R.L. Robinson, G.R. Young, Phys. Rev. C34 (1986) 858.

[42] : W.K. Wilson, W. Benenson, D.A. Cebra, J. Clayton, S. Howden, J. Karn, T. Li, C.A. Ogilvie, A. Vander Molen, G.D. Westfall, J.S. Winfield, B. Young, A. Nadasen, Phys. Rev. C41 (1990) R1881.

[43] : A. Buta, M. Petrovici, I. Legrand, D. Moisa, V. Simion and the FOPI Collaboration, GSI report 95-1 (1995) p. 57.

[44] : W.M. Zhang, R. Madey, M. Elaasar, J. Schambach, D. Keane, B.D. Anderson, A.R. Baldwin, J. Cogar, J.W. Watson, G.D. Westfall, G. Krebs, H. Wieman, Phys. Rev. C42 (1990) R491.

[45] : W.K. Wilson, W. Bauer, D.A. Cebra, M. Cronqvist, D. Krofcheck, R. Lacey, T. Li, A. Nadasen, E. Norbeck, T. Reposeur, A. Vander Molen, C.A. Ogilvie, G.D. Westfall, J.S. Winfield, J. Yee, Phys. Rev. C51 (1995) 3136.

[46] : R. Popescu, J.C. Angélique, G. Auger, G. Bizard, R. Brou, A. Buta, C. Cabot, E. Crema, D. Cussol, Y. El Masri, P. Eudes, M. Gonin, K. Hagel, Z.Y. He, A. Kerambrun, C. Lebrun, J.P. Patry, A. Péghaire, J. Péter, R. Régimbart, E. Rosato, F. Saint-Laurent, J.C. Steckmeyer, B. Tamain, E. Vient, R. Wada, Phys. Lett. B331 (1994) 285.

[47] : J.C. Angélique, R. Popescu, G. Auger, G. Bizard, R. Brou, A. Buta, C. Cabot, E. Crema, D. Cussol, Y. El Masri, P. Eudes, M. Gonin, K. Hagel, Z.Y. He, A. Kerambrun, C. Lebrun, J.P. Patry, A. Péghaire, J. Péter, R. Régimbart, E. Rosato, F. Saint-Laurent, J.C. Steckmeyer, B. Tamain, E. Vient, R. Wada, Nucl. Phys. A583 (1995) 543.

[48] : J. Ritman for the FOPI collaboration, Nucl. Phys. (Proc. Suppl.) B44 (1995) 708.

Figure captions

figure 1 : FOPI phase I acceptance in the ($P_0^{\perp}$, y_0) plane for Au on Au collisions at 250 AMeV.

figure 2 : Correlation between the impact parameter and ERAT (left part), PM (right part), obtained from IQMD calculations (HM parametrization), for Au on Au collisions at 400 AMeV. The error bars correspond to the RMS-widths of the distributions.

figure 3 : Azimuthal distributions obtained for Au + Au collisions at 800 AMeV. The top part of the figure shows the azimuthal distributions of Z = 2 particles in three different ERAT bins and the bottom part shows the azimuthal distributions of different Z for the ERAT2 selection. The spectra are accumulated for particles with $-0.15 < y_0 < 0.15$ and $0.06 < P_0^{\perp} < 0.48$. The curves correspond to Fourier series fits.

figure 4 : R_N versus the PM selection for proton-like particles selected with $-0.15 < y_0 < 0.15$ and $0.06 < P_0^{\perp} < 0.48$ and emitted in Au on Au collisions at 400 AMeV.

figure 5 : R_N versus the charge of fragments selected with $-0.15 < y_0 < 0.15$ and $0.06 < P_0^{\perp} < 0.48$ for Au on Au collisions at 250 AMeV. The PM3 cut is applied to these events.

figure 6 : R_N versus the bombarding energy for different fragments selected with $-0.15 < y_0 < 0.15$ and $0.06 < P_0^{\perp} < 0.48$ and emitted in Au on Au collisions. The ERAT2 cut is applied to these events.

figure 7 : R_N versus $P^{\perp}/A$ (left part) and $P_0^{\perp}$ (right part) for midrapidity ($-0.15 < y_0 < 0.15$) Z = 2 fragments emitted in Au on Au collisions between 150 and 800 AMeV and selected with the ERAT2 condition.

figure 8 : Azimuthal distributions for midrapidity ($-0.1 < y_0 < 0.1$) Z = 2, 3, 4 particles from

Au on Au collisions at an impact parameter selected by PM4. Each raw corresponds to the incident energy shown in the last column. The meaning of the fitted curves is explained in the text.

figure 9 : Incident energy dependence of R_N for midrapidity ($-0.1 < y_0 < 0.1$) Z = 2 (full circles), Z = 3 (full triangles) and Z = 4 (full squares). The dotted, dashed and full curves represent the result of a second order polynomial fit to the Z = 2, Z = 3 and Z = 4 experimental R_N ratio, respectively and the corresponding arrows indicate the position of the transition energy. Empty circles and empty triangles show the result of a similar analysis for data generated with IQMD, HM and SM respectively, for Z = 2, filtered with the experimental device.

Table caption

table 1 : Mean values and standard deviations of the impact parameter obtained from IQMD calculations (HM parametrization) for various ERAT and PM classes at 400 AMeV.

centrality selections	b (fm)
ERAT2	7.4 ± 1.8
ERAT3	5.5 ± 1.8
ERAT4	3.9 ± 1.1
ERAT5	2.3 ± 1.0
PM3	7.0 ± 1.1
PM4	4.1 ± 1.6
PM5	3.2 ± 1.1

table 1

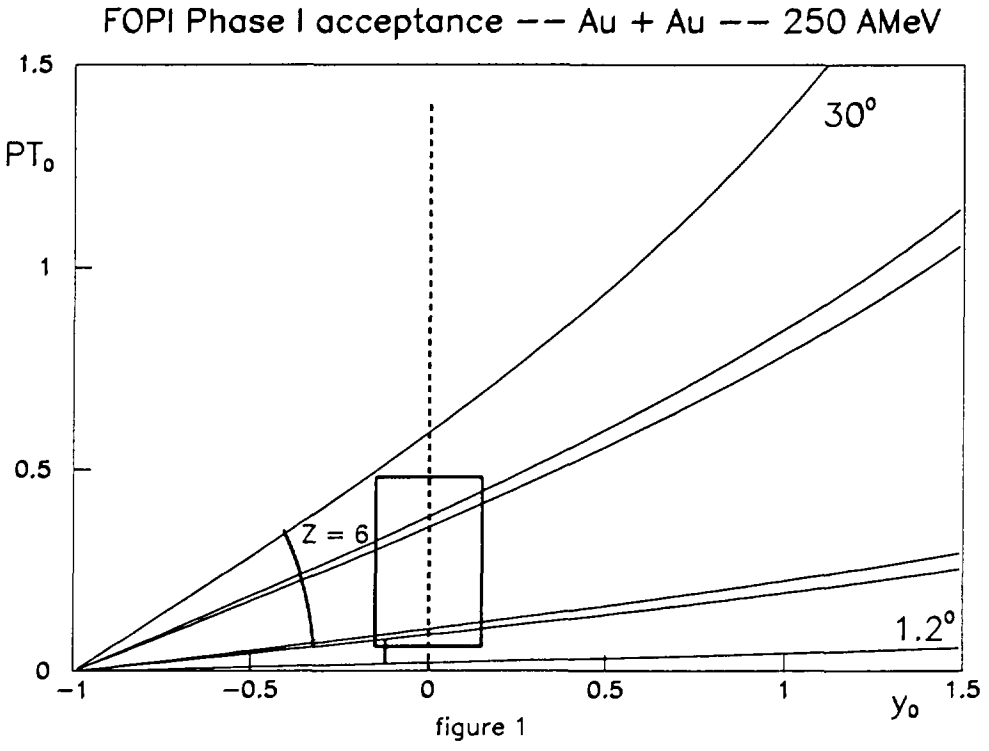
FOPI Phase I acceptance -- Au + Au -- 250 AMeV
1.5
PT0
1
0.5
0
30°
Z = 6
1.2°
−1
−0.5
0
0.5
1
1.5
y0
figure 1

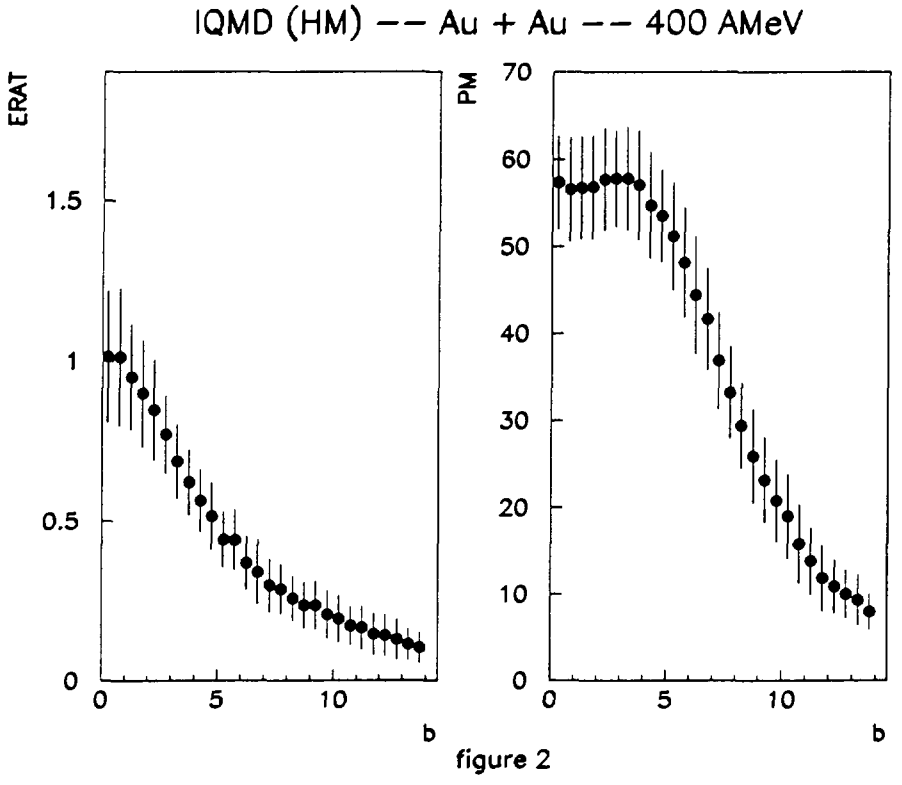
IQMD (HM) -- Au + Au -- 400 AMeV
ERAT
1.5
1
0.5
0
0
5
10
b
PM
70
60
50
40
30
20
10
0
0
5
10
b

figure 2

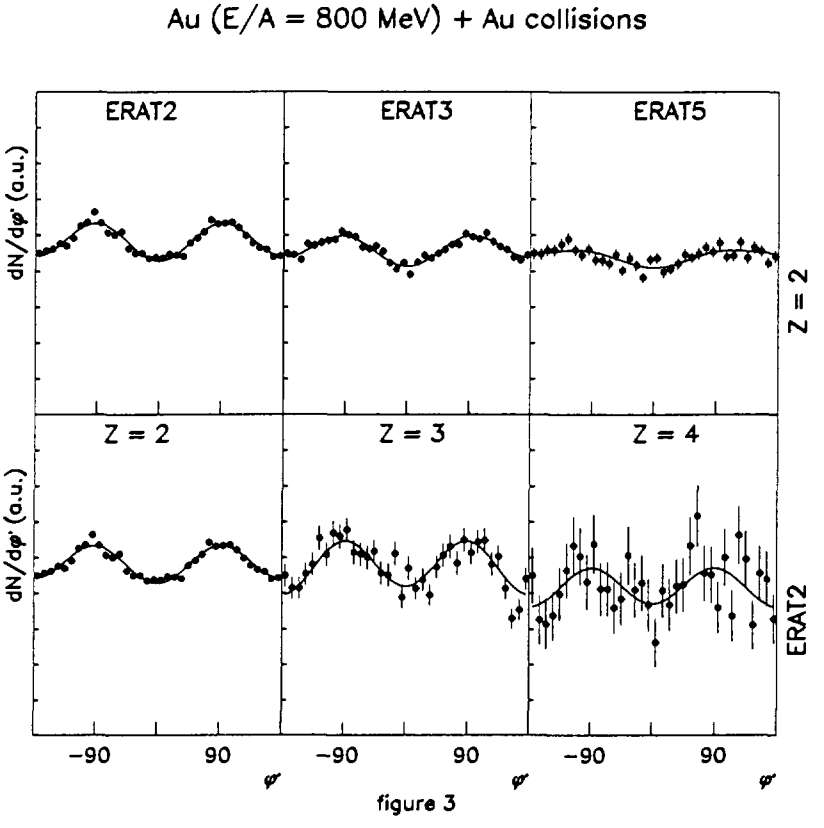
Au (E/A = 800 MeV) + Au collisions
ERAT2
ERAT3
ERAT5
Z = 2
Z = 2
Z = 3
Z = 4
ERAT2
dN/dφ' (a.u.)
dN/dφ' (a.u.)
−90
90
−90
90
−90
90
φ'
φ'
φ'

figure 3

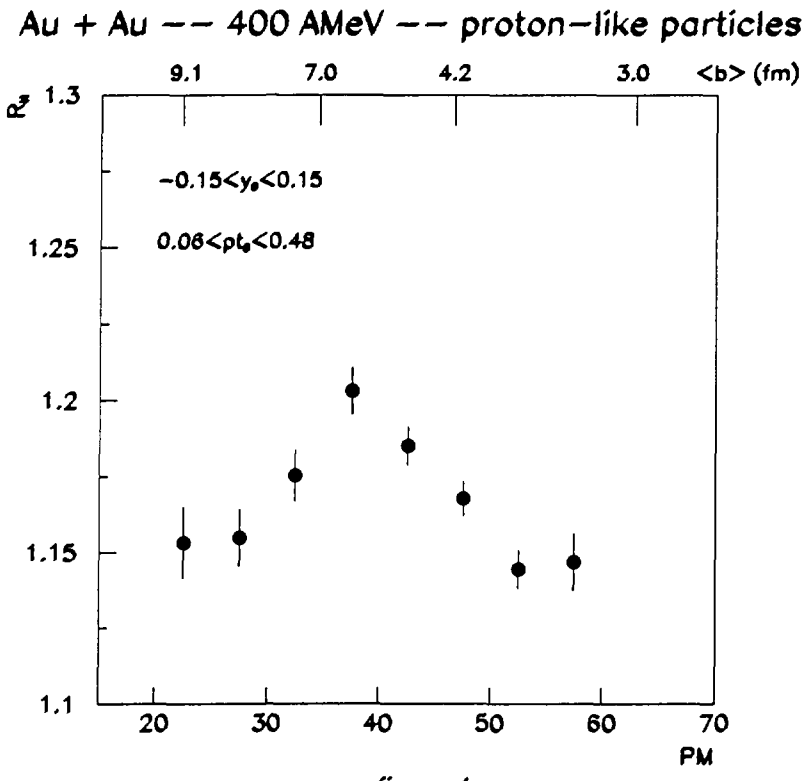
Au + Au -- 400 AMeV -- proton-like particles
9.1
7.0
4.2
3.0
<b> (fm)
α_z
1.3
1.25
1.2
1.15
1.1
$-0.15<y_0<0.15$
$0.06<pt_0<0.48$
20
30
40
50
60
70
PM

figure 4

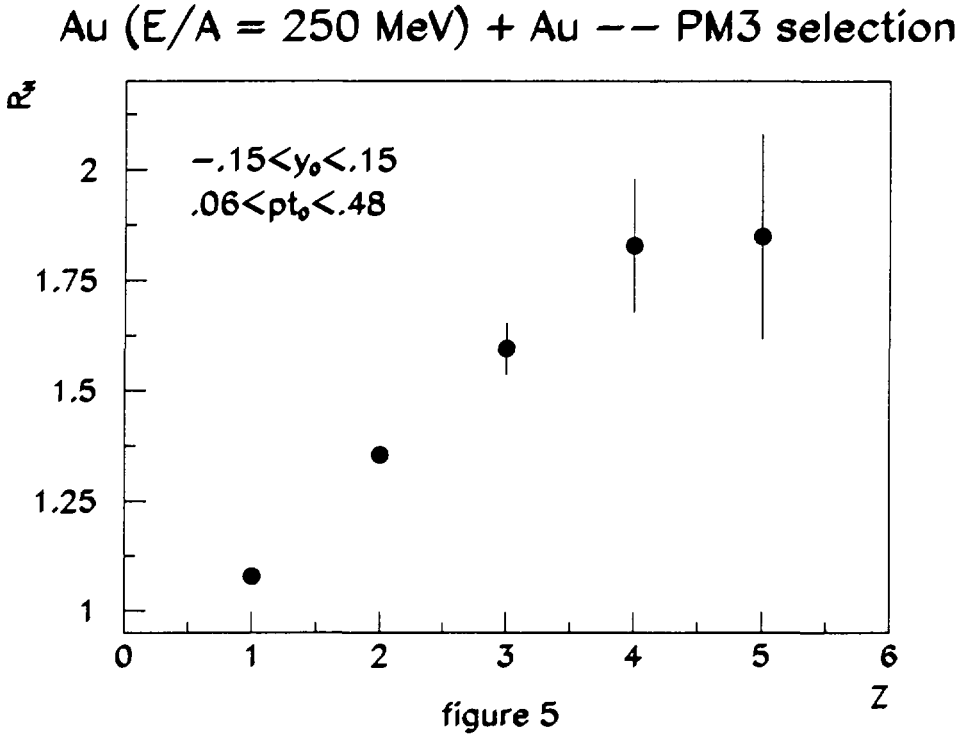
Au (E/A = 250 MeV) + Au -- PM3 selection
R
2
1.75
1.5
1.25
1
−.15<y₀<.15
.06<pt₀<.48
0
1
2
3
4
5
6
Z

figure 5

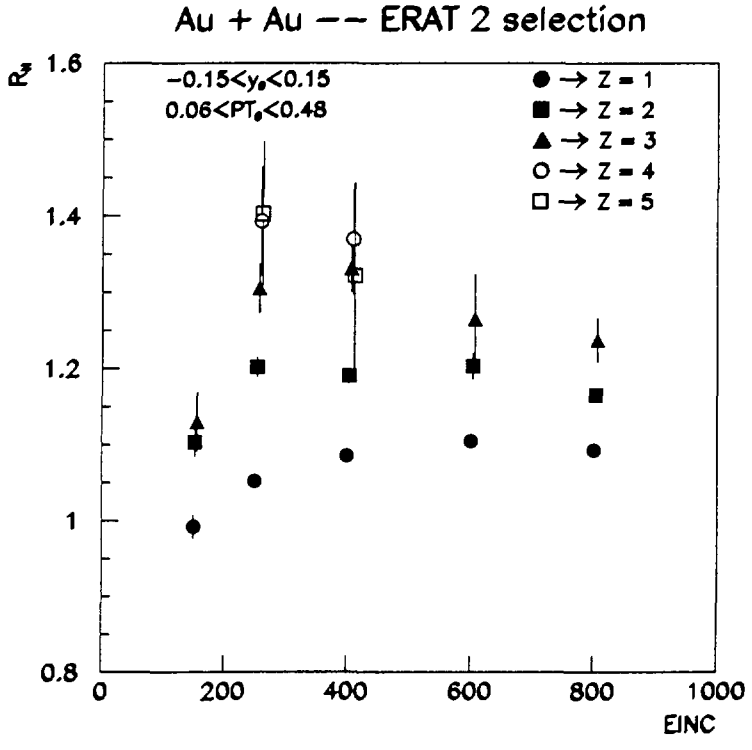
Au + Au -- ERAT 2 selection
R_2
1.6
1.4
1.2
1
0.8
$-0.15<y_0<0.15$
$0.06<PT_0<0.48$
● → Z = 1
■ → Z = 2
▲ → Z = 3
○ → Z = 4
□ → Z = 5
0
200
400
600
800
1000
EINC

figure 6

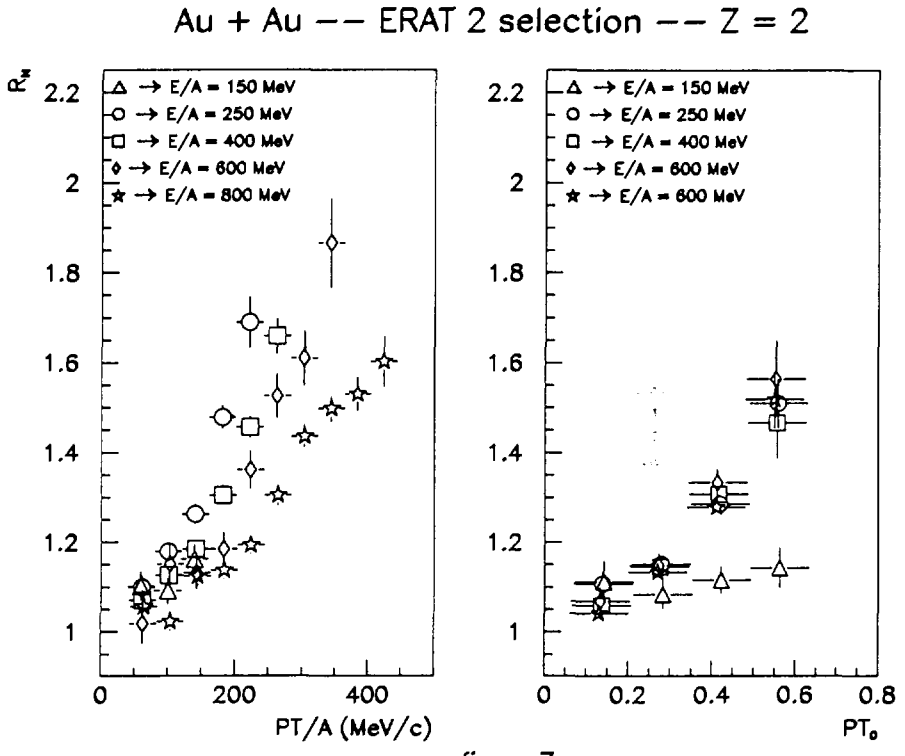
Au + Au -- ERAT 2 selection -- Z = 2
α*
2.2
2
1.8
1.6
1.4
1.2
1
0
200
400
PT/A (MeV/c)
Δ → E/A = 150 MeV
○ → E/A = 250 MeV
□ → E/A = 400 MeV
◊ → E/A = 600 MeV
☆ → E/A = 800 MeV
0.2
0.4
0.6
0.8
PT₀

figure 7

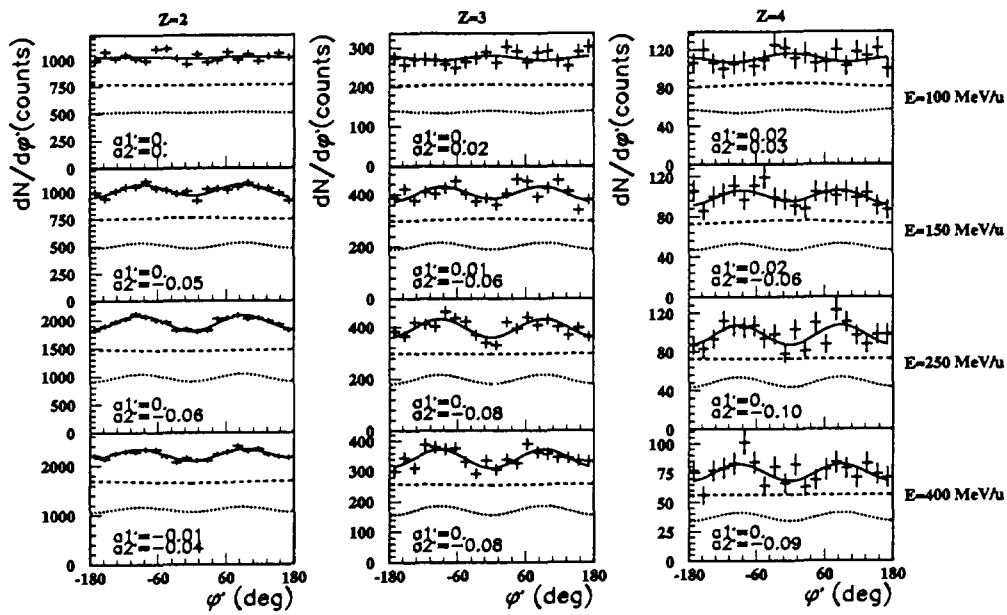
Au+Au,PM4
Z=2
Z=3
Z=4
dN/dφ'(counts)
φ' (deg)
E=100 MeV/u
E=150 MeV/u
E=250 MeV/u
E=400 MeV/u
a1=0
a2=0
a2=-0.05
a2=-0.06
a1=-0.01
a2=-0.04
a2=0.02
a2=-0.06
a2=-0.08
a1=0.02
a2=0.03
a2=-0.10
a2=-0.09

figure 8

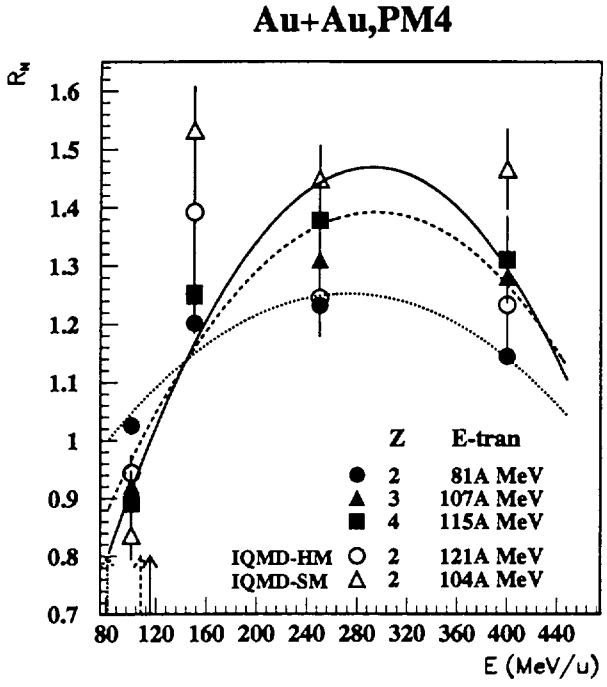
Au+Au,PM4
R_M
1.6
1.5
1.4
1.3
1.2
1.1
1
0.9
0.8
0.7
80 120 160 200 240 280 320 360 400 440
E (MeV/u)
Z E-tran
2 81A MeV
3 107A MeV
4 115A MeV
IQMD-HM 2 121A MeV
IQMD-SM 2 104A MeV

figure 9